Environ Fluid Mech (2007) 7:495–508
DOI 10.1007/s10652-007-9038-3

ORIGINAL ARTICLE

Advanced post-processing and correlation analyses in high-velocity air–water flows

Hubert Chanson · Giovanna Carosi

Received: 4 September 2007 / Accepted: 6 September 2007 / Published online: 2 October 2007

Abstract The interest in air–water flows has not diminished in recent years, but it is accompanied by frequent citations of early, sometimes outdated articles. A basic issue is the inadequate, incomplete interpretation of air–water flow instrumentation by hydraulic engineers and researchers. This article comments on high-velocity air–water flow measurements by means of intrusive phase detection probes. This article focus on the bubbly flow structure of high-velocity air–water flow based upon measurements by means of intrusive phase detection probes. It is shown that some advanced post-processing techniques may yield expanded information on the air–water turbulent flow properties and bubbly flow structures. The outcomes demonstrate simple techniques in high-velocity air–water flow analysis.

Keywords Signal processing · Phase-detection probes · High-velocity air–water flows · Hydraulic structures

1 Introduction

In steep rivers, mountainous streams and spillways, "white waters" are commonly observed. The air entrainment induces a drastic change in the fluid density and its distribution within the flow that have direct implications in terms of sediment ad turbulent processes. For example, in a flow with mean void fraction of 50%, the term (**s**-1) equals 4.3 compared to 1.65 in clear-water, where **s** is the ratio of the quartz particle density to fluid density. Air–water flows have been studied recently compared to classical fluid mechanics [5,7]. The interest in air–water flows is evidenced by the number of associated papers published in the IAHR Journal of Hydraulic Research, the International Journal of Multiphase Flow and the ASME Journal of Fluids Engineering. It is accompanied by frequent citations of early, sometimes outdated articles while some fundamental works are too often ignored [e.g. 1,2]. All these suggest little progress in the past four decades despite exaggerated claims. A basic issue

H. Chanson (✉) · G. Carosi
Division of Civil Engineering, The University of Queensland, Brisbane QLD 4072, Australia
e-mail: h.chanson@uq.edu.au

is the inadequate, incomplete interpretation of air–water flow instrumentation by hydraulic engineers and researchers that derives from crude signal processing methods, despite a few critical contributions [4,6].

Herein the writers demystify the data processing of air–water flow measurements. They show some simple analyses yielding some expanded information on the air–water flow properties and turbulence structures. Some novel methods yield further information on the air–water microscopic flow properties and air–water bubbly structures. This is illustrated with recent applications to air entrainment in hydraulic jumps and free-surface aeration in skimming flows on stepped spillways [10,11].

2 Phase detection probes

In high-velocity air–water flows, air entrainment is always substantial and classical measurement devices (e.g. Pitot tube, LDV) are adversely affected by the entrained bubbles. For void fractions between 5 and 95%, the most robust instrumentation is the needle-shaped phase detection probe: optical fibre probes and conductivity/resistivity probe. The intrusive probe is designed to pierce the bubbles and droplets (Fig. 1). There are two basic probe designs: single-tip probe and double-tip probe. A typical conductivity probe sensor consists of a fine sharpened rod coated with non-conductive resin and set into a stainless steel surgical needle acting as the second electrode. With a double-tip probe, the probe sensors are separated by a known streamwise distance Δx. Each sensor must be excited by a high-frequency response electronic system. Figure 2 shows some typical signal outputs of two single-tip probes side-by-side ($\Delta z = 3.6$ mm). The time-variation of the voltage output has a "square-wave" shape. Each steep drop of the signal corresponds to an air bubble pierced by the probe tip. The signal is theoretically rectangular, but the probe response is not square because of the finite size of the tip, the wetting/drying time of the interface covering the tip and the response time of the probe and electronics.

Phase-detection probes are very sensitive devices and they are susceptible to a number of problems. A quality control procedure must be systematically applied [22, pp. 70–72]. Specifically, the probe signals may exhibit some long-term signal decays often induced by probe tip contamination, short-term signal fluctuations caused by debris and water impurities, electrical noise and non-representative samples. Although most quality control procedures can be automatised, it must be stressed that human supervision and intervention are essential to validate each quality control step. Lastly, the effect of probe sensor size on the air–water flow properties was rarely tested but by Chanson and Toombes [12] and Carosi and Chanson [3] in skimming flows on stepped spillways. The results demonstrated that the probe sensor size has a major effect on the bubble count rate and bubble chord size data. Some comparative results between 0.025 mm and 0.35 mm sensor sizes showed consistently larger measured count rates and a broader range of bubble/droplet sizes with the 0.025 mm probe sensor. Simply, the sensor size must be smaller than the smallest bubble/droplet dimensions.

3 Signal processing

The measurement principle of phase-detection intrusive probes is based upon the difference in optical index or electrical resistivity between air and water. The intrusive probe sensor is designed to pierce the bubbles and droplets. That is, the probe sensor must be sharpened and it must ideally face the stream of incoming bubbles as shown in Fig. 1A. A typical probe

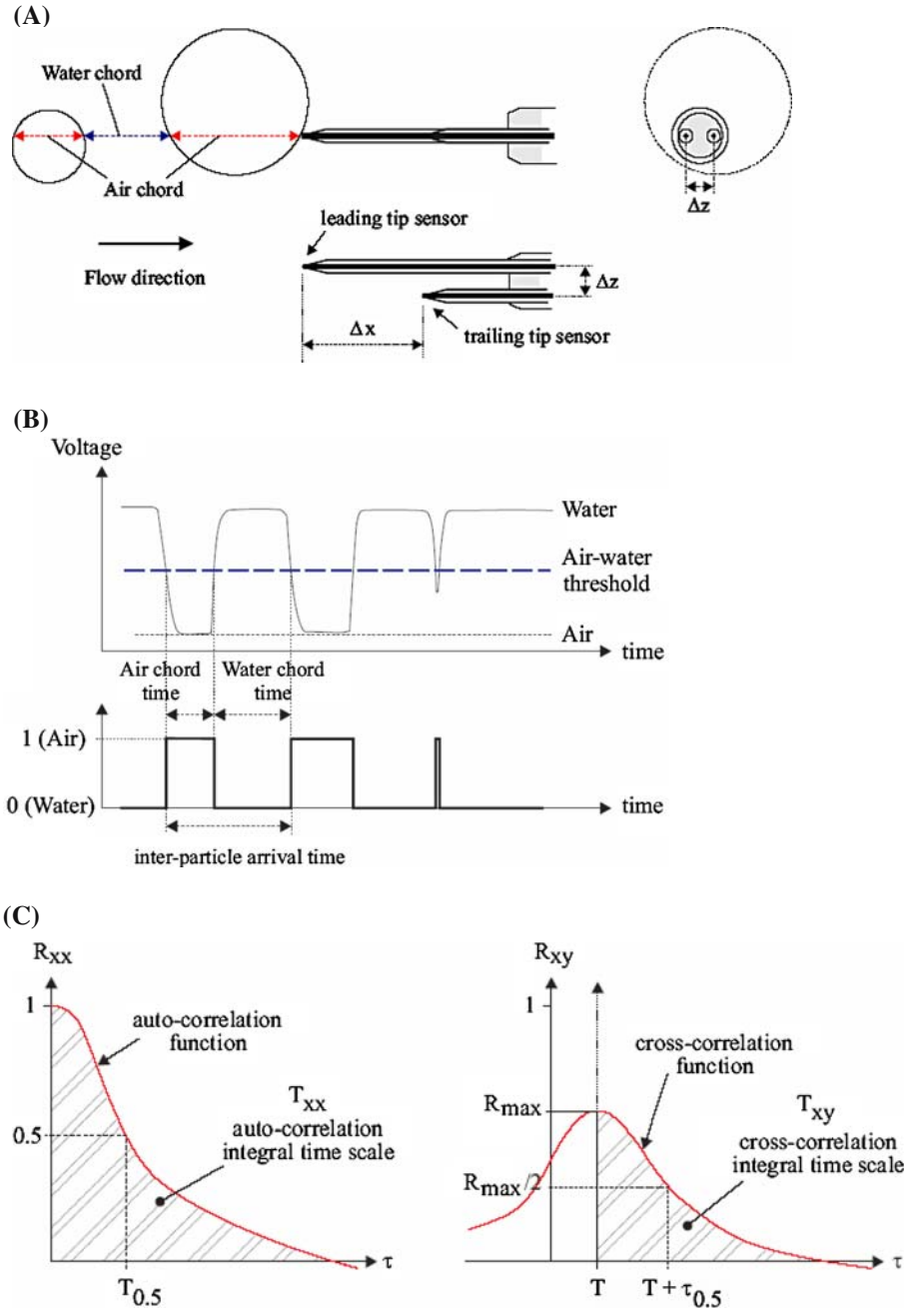

Fig. 1 Dual sensor phase detection probe. (**A**) Definition sketch, (**B**) Signal output from the leading sensor, and (**C**) Correlation functions

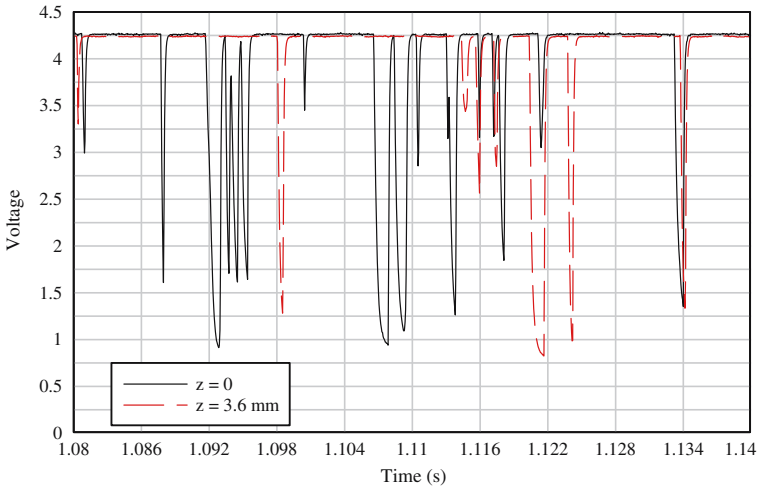

Fig. 2 Signal outputs of two single-tip conductivity probes side-by-side ($\Delta z = 3.6$ mm) in skimming flow—$d_c/h = 1.15$, $Re = 4.6$ E+5, $h = 0.1$ m, $\theta = 22°$, Step edge 10, $y = 0.022$ m, $C = 0.114$, $F = 117$ Hz, $(R_{xy})_{max} = 0.41$

signal output is shown in Fig. 2. The signal processing may be conducted on the raw signal output (e.g. Fig. 2) and on a thresholded "square wave" signal.

A thresholded signal analysis relies upon some arbitrary discrimination between the two phases. The technique may be based upon single or multiple thresholds, or some signal pattern recognition. The resulting square-wave signal yields the instantaneous void fraction C: $C = 0$ in water and $C = 1$ in air (Fig. 1B). It is used to calculate the time-averaged void fraction, bubble count rate, the air/water chord times, the bubble/droplet chord lengths and their statistical moments (mean, median, std, skewness, kurtosis), and the streamwise particle grouping analysis. In high-velocity flows, the most robust discrimination technique is the single threshold technique with a threshold set at about 45–55% of the air–water voltage range [21,22, pp. 55–56].

The signal processing of the raw probe outputs is typically used for some correlation analyses. These yield the time-averaged interfacial velocity, the turbulence intensity, the auto-correlation and cross-correlation integral time and length scales, the air–water integral length and time scales (see below). A further level of signal analysis is the spectral analyses (e.g. [17]).

3.1 Basic air–water flow properties

The time-averaged void fraction C is the proportion of time that the probe tip is in the air. Although past experiences showed that the probe orientation with the flow direction had little effect on the void fraction accuracy, the phase-detection probes are designed to pierce the bubbles/droplets with minimum interference and the probe sensor should face the bubbles/droplets as sketched in Fig. 1A.

The bubble count rate F is the number of bubbles impacting the probe tip per second. Note the relationship between bubble count rate and void fraction. Experimental data showed a pseudo-parabolic relationship:

$$\frac{F}{F_{\max}} = 4 \times C \times (1 - C) \tag{1}$$

where $F_{\max}$ is the maximum bubble frequency. Toombes [22] demonstrated the theoretical validity and he proposed a more general extension [22,23]. Another reasoning yields a similar relationship. The bubble count rate is proportional to the fluctuations of the instantaneous void fraction that is either 0 or 1. Simple considerations show that its variance C_{rms}^2 equals $C \times (1 - C)$ where C is the time-averaged void fraction. Hence the bubble count rate must satisfy: $F \propto C_{rms}^2 = C \times (1 - C)$.

3.2 Correlation analyses

When two or more phase detection probe sensors are simultaneously sampled, some correlation analyses may provide additional information on the bubbly flow structure. A well-known application is the use of dual tip probe to measure the interfacial velocity (Fig. 1). With large void fractions ($C > 0.10$), a cross-correlation analysis between the two probe sensors yields the time averaged velocity:

$$V = \frac{\Delta x}{T} \tag{2}$$

where T is the air–water interfacial travel time for which the cross-correlation function is maximum and Δx is the longitudinal distance between probe sensors (Fig. 1). Turbulence levels may be further derived from the relative width of the cross-correlation function:

$$Tu = 0.85 \times \frac{\sqrt{\tau_{0.5}^2 - T_{0.5}^2}}{T} \tag{3}$$

where $\tau_{0.5}$ is the time scale for which the cross-correlation function is half of its maximum value such as: $R_{xy}(T + \tau_{0.5}) = 0.5 \times R_{xy}(T)$, R_{xy} is the normalised cross-correlation function, and $T_{0.5}$ is the characteristic time for which the normalised auto-correlation function equals: $R_{xx}(T_{0.5}) = 0.5$ (Fig. 1). Physically, a thin narrow cross-correlation function ($(\tau_{0.5} - T_{0.5})/T << 1$) must correspond to little fluctuations in the interfacial velocity, hence a small turbulence level Tu. While Eq. 3 is not the true turbulence intensity u'/V, it is an expression of some turbulence level and average velocity fluctuations [14].

More generally, when two probe sensors are separated by a transverse or longitudinal distance Y, their signals may be analysed in terms of the auto-correlation and cross-correlation functions R_{xx} and R_{xy} respectively. Figure 3 shows two probe sensors separated by a transverse distance Y. Practically the original data set may be segmented because the periodogram resolution is inversely proportional to the number of samples and it could be biased with large data sets [19]. Basic correlation analysis results include the maximum cross-correlation coefficient $(R_{xy})_{\max}$, and the auto- and cross-correlation time scales T_{xx} and T_{xy} where:

$$T_{xx} = \int_{\tau=0}^{\tau=\tau(R_{xx}=0)} R_{xx}(\tau) \times \mathrm{d}\tau \tag{4}$$

$$T_{xy} = \int_{\tau=0}^{\tau=\tau(R_{xy}=0)} R_{xy}(\tau) \times \mathrm{d}\tau \tag{5}$$

where R_{xx} is the normalised auto-correlation function, τ is the time lag, and R_{xy} is the normalised cross-correlation function between the two probe output signals (Fig. 1C). The auto-correlation time scale T_{xx} represents the integral time scale of the longitudinal bubbly

Fig. 3 Photograph of two single-tip conductivity probes side-by-side in a hydraulic jump ($Fr_1 = 7.9$, $\rho_w \times V_1 \times d_1/\mu_w = 9.4$ E+4)—Flow from right to left

flow structure. It is a characteristic time of the eddies advecting the air–water interfaces in the longitudinal direction. The cross-correlation time scale T_{xy} is a characteristic time of the vortices with a length scale Y advecting the air–water flow structures. The length scale Y may be a transverse separation distance Δz or a streamwise separation Δx.

When identical experiments with two probes are repeated using different separation distances Y ($Y = \Delta z$ or Δx), an integral turbulent length scale may be calculated as:

$$L_{xy} = \int_{Y=0}^{Y=Y((R_{xy})_{max}=0)} (R_{xy})_{max} \times dY \tag{6}$$

The length scale L_{xy} represents a measure of the transverse/streamwise length scale of the large vortical structures advecting air bubbles and air–water packets. A turbulence integral time scale is:

$$T = \frac{1}{L_{xy}} \times \int_{Y=0}^{Y=Y((R_{xy})_{max}=0)} (R_{xy})_{max} \times T_{xy} \times dY \tag{7}$$

T represents the transverse/streamwise integral time scale of the large eddies advecting air bubbles.

Figure 4 presents some experimental results obtained in a hydraulic jump on a horizontal channel and in a skimming flow on a stepped channel. In both flow situations, the distributions of integral time scales showed a marked peak for $0.4 \leq C \leq 0.6$ (Fig. 4). Note that

Fig. 4 Dimensionless distributions of integral turbulent time and length scales in high-velocity air–water flows. (**A**) Dimensionless distributions of auto- and cross-correlation time scales $T_{xx} \times \sqrt{g/d_1}$ and $T_{xy} \times \sqrt{g/d_1}$ (transverse time, $Y = \Delta z = 10.5$ mm), and transverse integral turbulent length scale L_{xy}/d_1 in a hydraulic jump – $Fr_1 = 7.9$, $x - x_1 = 0.1$ m, $d_1 = 0.0245$ m [8]. (**B**) Dimensionless distributions of auto- and cross-correlation time scales $T_{xx} \times \sqrt{g/Y_{90}}$ and $T_{xy} \times \sqrt{g/Y_{90}}$ (longitudinal time scale, $Y = \Delta x = 9.6$ mm) in a skimming flow on a stepped chute—$d_c/h = 1.15$, $\rho_w \times V \times d/\mu_w = 1.2$ E+5, Step 10, $Y_{90} = 0.0574$ m, $h = 0.1$ m, $\theta = 22°$ [3]. (**C**) Dimensionless distributions of transverse integral turbulent length scale L_{xy}/Y_{90} in a skimming flow on a stepped chute—$d_c/h = 1.15$, $\rho_w \times V \times d/\mu_w = 1.2$ E+5, Step 10, $Y_{90} = 0.0598$ m, $h = 0.1$ m, $\theta = 22°$ [3] ▶

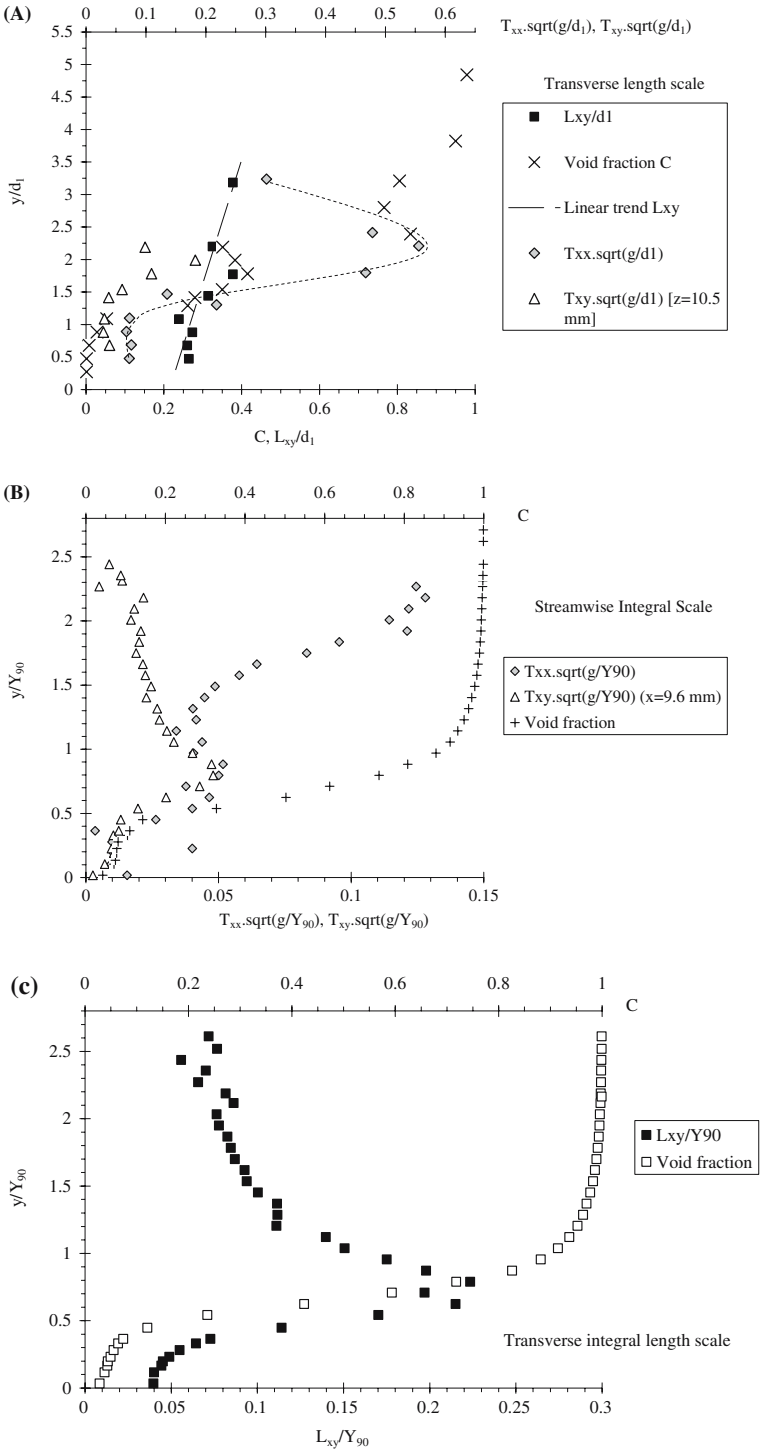
(A)
$T_{xx}.sqrt(g/d_1)$, $T_{xy}.sqrt(g/d_1)$
Transverse length scale
Lxy/d1
Void fraction C
Linear trend Lxy
Txx.sqrt(g/d1)
Txy.sqrt(g/d1) [z=10.5 mm]
y/d_1
C, L_{xy}/d_1
(B)
C
Streamwise Integral Scale
Txx.sqrt(g/Y90)
Txy.sqrt(g/Y90) (x=9.6 mm)
Void fraction
y/Y_{90}
$T_{xx}.sqrt(g/Y_{90})$, $T_{xy}.sqrt(g/Y_{90})$
(c)
C
Lxy/Y90
Void fraction
Transverse integral length scale
y/Y_{90}
L_{xy}/Y_{90}

Fig. 4A presents some transverse time scales T_{xy} while Fig. 4B shows some longitudinal time scales T_{xy}. The distributions of transverse integral length scales exhibited some marked differences that may reflect the differences in turbulent mixing and air bubble advection processes between hydraulic jump and skimming flows. Figure 4C shows the dimensionless turbulent length scale L_{xy}/Y_{90} in a skimming flow where Y_{90} is the distance normal to the pseudo-bottom formed by the step edges where $C = 0.90$.

4 Air/water chord distributions

In high-velocity air–water flows, most experimental studies present the distributions of time-averaged void fraction and time-averaged velocity. The void fraction and velocity are some gross parameters that do not describe the air–water structures, the bubbly flow micro-turbulence nor the interactions between entrained bubbles and turbulent shear. Further signal processing may provide additional characteristics on the longitudinal flow structure and bubble clustering.

With a single-tip conductivity probe, a basic signal processing yields the air/water chord times and their distribution. The air/water chord times are defined as the time spent by the air/water phase on the probe sensor. Bubble chord times are calculated from the thresholded signal [10]. Statistical analyses of chord time distributions yield the median chord time, standard deviation, skewness and kurtosis of both air and water chord times. Inter-particle arrival times may be also calculated and analysed (see below).

Using the single-tip conductivity probe, the chord time results may be presented in terms of pseudo-bubble/droplet chord sizes *ch* defined as:

$$ch = U_w \times t_{ch} \tag{8}$$

where t_{ch} is the air/water chord time, U_w is the mean flow velocity defined as: $U_w = q_w/d$, q_w is the flow rate per unit width and d is the equivalent clear-water depth defined as:

$$d = \int_0^{Y_{90}} (1 - C) \times \mathrm{d}y \tag{9}$$

with y the distance normal to the flow direction and Y_{90} the characteristic distance where the void fraction C equals 0.90. The pseudo chord size (Eq. 8) is not equal to the air/water chord length because the local interfacial velocity V may differ from the mean flow velocity U_w. But some detailed comparisons in plunging jet flows and skimming flows on a stepped chute showed that Eq. 8 overestimated the air/water chord sizes by 2–10% in average for $0 \leq C \leq 0.97$ [3,9].

With a double-tip probe, the signal processing yields the air/water chord lengths. The chord size measurement is not a bubble/droplet diameter, but a characteristic streamwise air/water size as sketched in Fig. 1A. Figure 5 presents typical results of air/water chord size probability distribution functions in a skimming flow on a stepped chute. The probability distribution functions of chord sizes are analysed in terms of bubble chords in the bubbly flow ($C < 0.3$) and in terms of droplet chords in the spray region ($C > 0.7$). Figure 5 shows some normalised chord size distributions. For each graph, the histogram columns represent each the probability of chord size in a 0.5 mm chord interval. For example, the probability of bubble chord from 1 to 1.5 mm is represented by the column labelled 1 mm. Chord sizes larger than 15 mm are regrouped in the last column (>15). Note that the caption and legend provide the local air–water flow properties (C, F) and probe details.

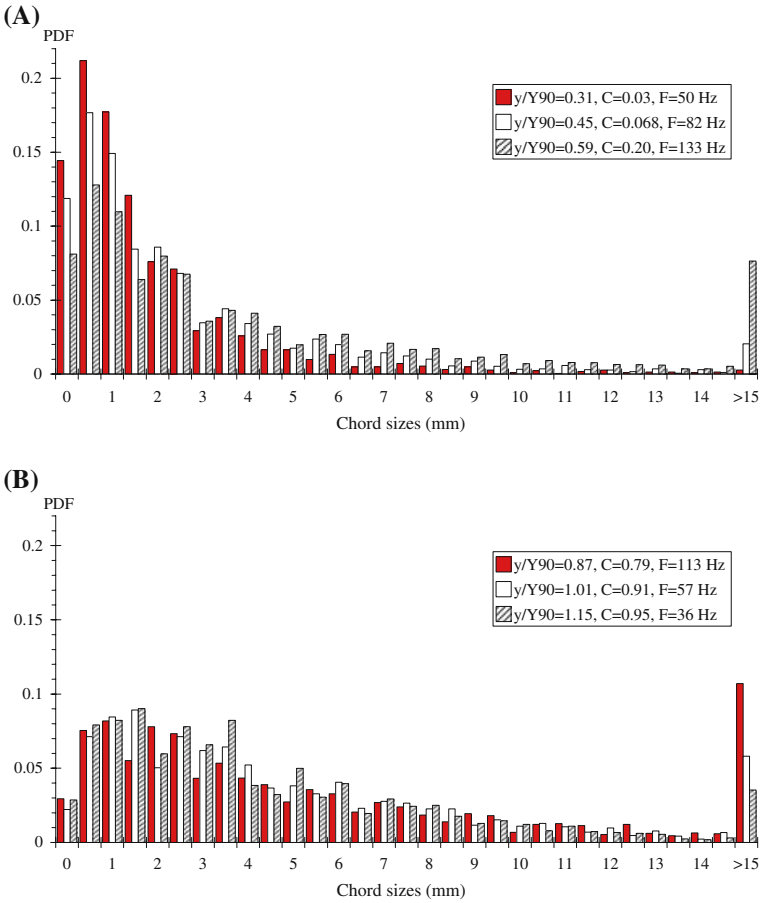

Fig. 5 Probability distribution functions of chord sizes in skimming flows: $d_c/h = 1.45$, Step 10, double-tip probe ($\emptyset = 0.25$ mm, $\Delta x = 7.0$ mm). (**A**) Bubble chord size data ($C < 0.3$) and (**B**) Droplet chord size data ($C > 0.7$)

5 Structure of bubbly flows

5.1 Streamwise particle grouping

With modern phase-detection intrusive probes, some simple signal processing yields the basic statistical moments of air and water chords as well as the probability distribution functions of chord times/sizes. Most experimental results demonstrated a broad spectrum of bubble chords in turbulent shear flows. The range of bubble chord lengths extended over several orders of magnitude including at low void fractions. The distributions of bubble chords were skewed with a preponderance of small bubbles relative to the mean (Fig. 5A). The probability distribution functions of bubble chords tended to follow a log-normal and gamma distributions. Similar findings were observed in a variety of flows encompassing hydraulic jumps, plunging jets, dropshaft flows and high-velocity open channel flows.

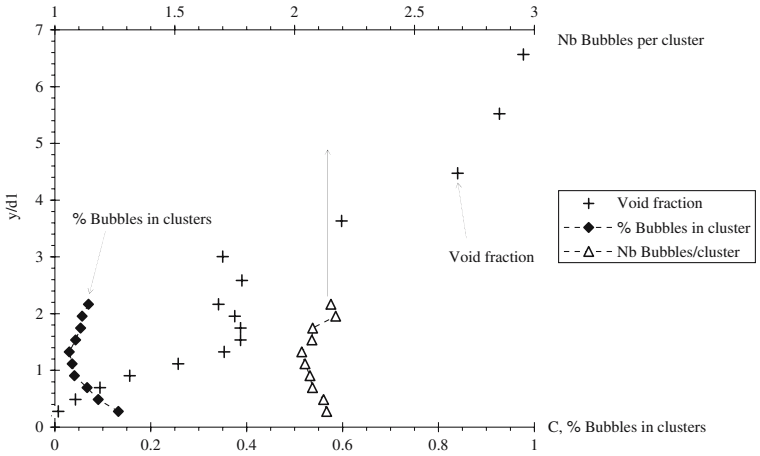

Fig. 6 Bubble clustering in the bubbly flow region of a hydraulic jump: percentage of bubbles in clusters, average number of bubbles per cluster and void fraction—Cluster criterion: water chord time <10% median water chord time—$Fr_1 = 8.5$, $\rho_w \times V_1 \times d_1/\mu_w = 9.8$ E+4, $x - x_1 = 0.3$ m, $d_1 = 0.024$ m [8]

In addition, a thorough signal processing may provide some information on the streamwise structure of the air–water flow including bubble clustering. A concentration of bubbles within some relatively short intervals of time may indicate some clustering while it may be instead the consequence of a random occurrence. The study of particle clustering events is relevant to infer whether the formation frequency responds to some particular frequencies of the flow.

One method is based upon the analysis of the water chord between two adjacent air bubbles. If two bubbles are closer than a particular length scale, they can be considered a group/cluster of bubbles. The characteristic water length scale may be related to the water chord statistics: e.g., a bubble cluster may be defined when the water chord was less than a given percentage of the mean water chord. Another criterion may be related to the leading particle size itself, since particles within that distance are in the near-wake of and may be influenced by the leading particle.

Typical results may include the percentage of bubbles in clusters, the number of clusters per second, and the average number of bubbles per cluster. Extensive experiments in open channels, hydraulic jumps and plunging jets suggested that the outcomes were relatively little affected by the cluster criterion selection [9,13,18]. Most results indicated that the longitudinal structure of turbulent flows was characterised by about 10–30% of bubbles travelling as parts of a group/cluster, with a very large majority of clusters comprising of two bubbles only. The experimental experience suggested further that a proper cluster analysis requires a high-frequency scan rate for a relatively long scan duration. However the analysis is restricted to the longitudinal distribution of bubbles and does not take into account particles travelling side by side.

A typical result is presented in Fig. 6 based upon measurements in the advective diffusion region of a hydraulic jump. Figure 6 shows the vertical distribution of the percentage of bubbles in clusters (lower horizontal axis) and average number of bubbles per cluster (upper horizontal axis) in the hydraulic jump shear layer. The void fraction distribution is also shown for completeness. The criterion for cluster existence was a water chord less than 10% of the median water chord. For this example, about 5–15% of all bubbles were part of a cluster structure and the average number of bubbles per cluster was about 2.1.

6 Inter-particle arrival time analysis

For a dispersed phase, a complementary approach is based upon an inter-particle arrival time analysis. The inter-particle arrival time is defined as the time between the arrivals of two consecutive bubbles recorded by a probe sensor fixed in space (Fig. 1B). In other words, it is the time between two successive water-to-air interfaces. The distribution of inter-particle arrival times provides some information on the randomness of the structure. Random dispersed flows are those whose inter-particle arrival time distributions follow inhomogeneous Poisson statistics assuming non-interacting point particles [15,20]. In other words, an ideal dispersed flow is driven by a superposition of Poisson processes of bubble sizes, and any deviation from a Poisson process indicates some unsteadiness and particle clustering. That is, the inter-particle time distribution function in steady-random dispersed flows is:

$$f(t) = \frac{\lambda \times (T_{scan} - t) \times \exp(-\lambda \times t)}{\lambda \times T_{scan} - 1 + \exp(-\lambda \times T_{scan})} \quad (10)$$

where t is the interparticle arrival time, T_{scan} is the sampling duration (herein 45 s), $\lambda = N_{ab}/T_{scan}$ and N_{ab} is the number of particles [20].

Equation (10) describes an ideal dispersed flow driven by a superposition of Poisson processes of bubble sizes assuming non-interacting particles. Any deviation from a Poisson process indicates some unsteadiness and particle clustering, and the degree of non-random particle clustering may be quantified by Chi-square tests. In practice, the analysis is conducted by breaking down the air–water flow data into narrow classes of particles of comparable sizes that are expected to have the same behaviour [16]. A simple means consists in dividing the bubble/droplet population in terms of the air/water chord time. The inter-particle arrival time analysis may provide some information on preferential clustering for particular classes of particle sizes.

Some results in terms of inter-particle arrival time distributions are shown in Fig. 7 for the same flow conditions and at the same cross-section as the data presented in Fig. 6. Figure 7 presents some inter-particle arrival time results for two chord time classes (0–0.5 msec and 3–5 msec). For each class of bubble sizes, a comparison between data and Poisson distribution gives some information on its randomness. For example, Fig. 7A shows that the data for bubble chord times below 0.5 msec did not experience a random behaviour because the experimental and theoretical distributions differed substantially in shape. The second smallest inter-particle time class (0.5–1 msec) had a population that was 2.5 times the expected value or about 11 standard deviations too large. Such a finding was not seen for medium-sized bubbles with chord times between 3 and 5 msec (Fig. 7B). This indicates that there was a higher probability of having bubbles with shorter inter-particle arrival times, hence some bubble clustering occurred. Simply the smallest class of bubble chord times did not exhibit the characteristics of a random process.

7 Conclusion

In mountainous rivers and steep chutes, the high-velocity air–water flows are characterised by large amounts of entrained air, with void fractions commonly larger than 5–10%, and with ratios of interfacial velocity to bubble rise velocity greater than 10–20. The most reliable metrology in high-velocity air–water flows is the intrusive phase detection probe that was used in both laboratory and full-scale studies [1,2,6]. The probe sensor is designed to pierce bubbles and droplets. Some advanced signal processing is developed and the results yield new

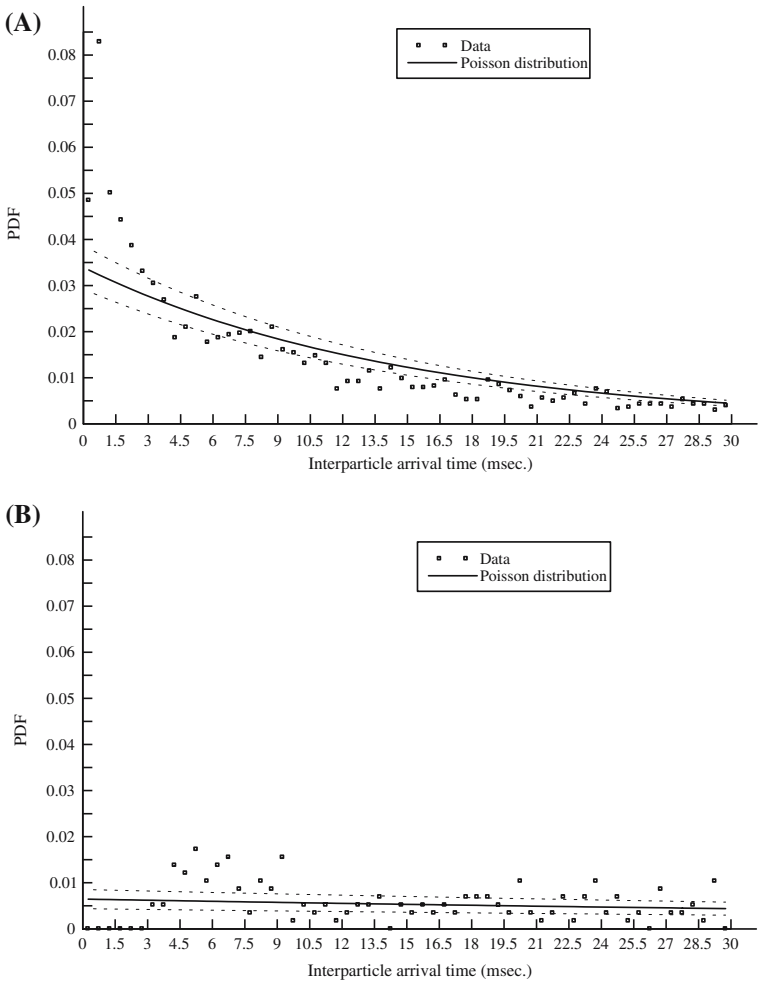

Fig. 7 Inter-particle arrival time distributions in the bubbly flow region of a hydraulic jump for different classes of air chord times - Comparison between data, Poisson distribution (Eq. 3, solid line) and expected deviations from the Poisson distribution (dashed lines)—$Fr_1 = 8.5$, $\rho_w \times V_1 \times d_1/\mu_w = 9.8$ E+4, $x - x_1 = 0.3$ m, $d_1 = 0.024$ m [8]. (**A**) Inter-particle arrival time distributions for bubble chord times between 0 and 0.5 msec, 3055 bubbles, $\chi^2 = 461$ and (**B**) Inter-particle arrival time distributions for bubble chord times between 3 and 5 msec, 581 bubbles, $\chi^2 = 110$

information on the air–water turbulent flow properties, bubbly flow structures and particle clustering.

There are two types of signal processing techniques. One is based upon the analysis of the thresholded signal. It is commonly used to calculate the void fraction, bubble count rate and particle size distributions. Another technique is based upon the raw signal processing. The most common application is the correlation analyses used to deduce the interfacial velocity, the turbulent intensity ad the air–water turbulent time and length scales.

In high-velocity flows, bubble chord distributions showed a broad range of chord times. The distributions were typically skewed with a preponderance of air/water chords smaller than the mean. An analysis of the longitudinal flow structure showed some bubble clustering in

the air–water turbulent shear flows. A complementary approach, based upon the inter-particle arrival time analysis, suggested some preferential bubble clustering for small bubble chord times within the investigated flow conditions. Altogether both approaches are complementary, but the inter-particle arrival time analyses give a greater insight into the range of particle classes affected by non-random clustering. This is believed to be a first step towards a better characterisation of air–water flow structures in turbulent shear flows, and the interactions between entrained air and turbulence.

References

1. Cain P, Wood IR (1981) Instrumentation for aerated flow on spillways. J Hyd Div ASCE 107(HY11):1407–1424
2. Cain P, Wood IR (1981) Measurements of self-aerated flow on a spillway. J Hyd Div ASCE 107(HY11): 1425–1444
3. Carosi G, Chanson H (2006) Air-water time and length scales in skimming flows on a stepped spillway. Application to the spray characterisation. Report No. CH59/06, Div of Civil Engineering, The University of Queensland, Brisbane, Australia, 142 pp
4. Chang KA, Lim HJ, Su CB (2003) Fiber optic reflectometer for velocity and fraction ratio measurements in multiphase flows. Rev Scientific Inst 74(7):3559–3565. Discussion: 2004, 75(1):284–286
5. Chanson H (1997) Air bubble entrainment in free-surface turbulent shear flows. Academic Press, London 401
6. Chanson H (2002) Air-water flow measurements with intrusive phase-detection probes. Can we improve their interpretation?. J Hyd Engrg ASCE 128(3):252–255
7. Chanson H (2004) Air-water flows in water engineering and hydraulic structures basic processes and metrology. In: Yazdandoost F, Attari J (eds) Proceedings of international conference on hydraulics of dams and river structures. Tehran, Iran, Invited Keynote lecture, Balkema Publication, The Netherlands, pp 3–16
8. Chanson H (2006) Air bubble entrainment in hydraulic jumps. Similitude and scale effects. Report No. CH57/05, Dept. of Civil Engineering, The University of Queensland, Brisbane, 119 pp
9. Chanson H, Aoki S, Hoque A (2006) Bubble entrainment and dispersion in plunging jet flows freshwater versus seawater. J Coast Res 22(3):664–677
10. Chanson H, Carosi G (2006a) Advanced post-processing and correlation analyses in high-velocity air-water flows. 1-Macroscopic properties. In: Montemor-o-Novo, Jorge Matos, Hubert Chanson (eds) Proceedings of the international junior researcher and engineer workshop on hydraulic structures (IJREWHS'06). Report CH61/06, Div. of Civil Engineering, The University of Queensland, Brisbane, Australia. December, pp 139–148, ISBN 1864998687
11. Chanson H, Carosi G (2006b) Advanced post-processing and correlation analyses in high-velocity air-water flows. 2-Microscopic properties. In: Montemor-o-Novo, Jorge Matos, Hubert Chanson (eds) Proceedings of the international junior researcher and engineer workshop on hydraulic structures (IJREWHS'06). Report CH61/06, Div. of Civil Engineering, The University of Queensland, Brisbane, Australia. December, pp 149–158, ISBN 1864998687
12. Chanson H, Toombes L (2002) Experimental study of gas-liquid interfacial properties in a stepped cascade flow. Environ Fluid Mech 2(3):241–263
13. Chanson H, Toombes L (2002) Air-water flows down stepped chutes turbulence and flow structure observations. Int J Multiphase Flow 28(11):1737–1761
14. Chanson H, Toombes L (2003) Strong interactions between free-surface aeration and turbulence in an open channel flow. Exp Thermal Fluid Sci 27(5):525–535
15. Edwards CF, Marx KD (1995) Multipoint statistical structure of the ideal spray, part I: fundamental concepts and the realization density. Atomization Sprays 5:435–455
16. Edwards CF, Marx KD (1995) Multipoint statistical structure of the ideal spray, part II: evaluating steadiness using the inter-particle time distribution. Atomization Sprays 5:435–455
17. Gonzalez CA (2005) An experimental study of free-surface aeration on embankment stepped chutes. Ph.D. thesis, Department of Civil Engineering, The University of Queensland, Brisbane, 240 pp
18. Gualtieri C, Chanson H (2004) Clustering process and interfacial area analysis in a large-size dropshaft. In: Mendes A, Rahman M, Brebbia CA (eds) Proceedings of 5th International Conference on advances in fluid mechanics AFM 2004 Lisbon, March 22–24. Advances in fluid mechanics, vol V. WIT Press, Southampton, pp 415–424

19. Hayes MH (1996) Statistical, digital signal processing and modeling. John Wiley, New York
20. Heinlein J, Fritsching U (2006) Droplet clustering in sprays. Exp Fluids 40(3):464–472
21. Herringe RA, Davis MR (1974) Detection of instantaneous phase changes in gas-liquid mixtures. J Phys E: Scientific Instruments 7:807–812
22. Toombes L (2002) Experimental study of air-water flow properties on low-gradient stepped cascades. Ph.D. thesis, Dept of Civil Engineering, The University of Queensland, Brisbane
23. Toombes L, Chanson H (2007) Surface waves and roughness in self-aerated supercritical flow. Environm Fluid Mech 5(3):259–270. doi:10.1007/s10652-007-9022-y